

Article

A New Method for Correcting the Deviation of a Middle Pier Tower of a Long-Span Intermediate Arch Bridge

Xiaojin Dong and Dan Ye *

State Key Laboratory of Mountain Bridge and Tunnel Engineering, Chongqing Jiaotong University, Chongqing 400074, China; 18943995727@163.com

* Correspondence: yedan@cque.edu.cn

Abstract: To control the deviation of a long-span concrete-filled steel tube (CFST) arch bridge during construction monitoring, a practical method for controlling tower deviation is studied and established. The form of construction of this bridge is an intermediate double-arch bridge, which differs from conventional bridges, thus requiring the urgent resolution of the issue of unbalanced middle piers. Therefore, the mechanical characteristics and construction process of an intermediate long-span, dual-coupled steel pipe arch bridge are meticulously examined by using a 1:10 scale model, with particular focus on discussing the deflection of the buckle tower during the installation of the arch rib segments. Construction control is implemented using a novel tower deflection control method that addresses unilateral torsion problems and difficulties in controlling the deflection of the tower. The model results are compared with the finite element analysis output, demonstrating that this new approach can resolve unbalanced tower deviations by maintaining absolute values within 0.5 mm. After correcting these deviations, the measured results from the model bridge tower align with the calculated analytical results and even surpass the theoretical expectations for tower deviation. This remarkable new method accurately resolves real-world bridge tower deviations.

Keywords: bridge engineering; arch bridge; tower deviation control; control method



Citation: Dong, X.; Ye, D. A New Method for Correcting the Deviation of a Middle Pier Tower of a Long-Span Intermediate Arch Bridge. *Buildings* **2023**, *13*, 2498. <https://doi.org/10.3390/buildings13102498>

Academic Editor: Carmelo Gentile

Received: 10 August 2023

Revised: 20 September 2023

Accepted: 28 September 2023

Published: 30 September 2023



Copyright: © 2023 by the authors. Licensee MDPI, Basel, Switzerland. This article is an open access article distributed under the terms and conditions of the Creative Commons Attribution (CC BY) license (<https://creativecommons.org/licenses/by/4.0/>).

1. Introduction

With the wide application of steel pipe concrete arch bridges, its forms of construction are becoming more diversified [1]. The span of the bridge has developed from just over 100 m in the beginning to nearly 600 m at present [2,3]. The design of a concrete-filled steel tube (CFST) arch bridge is usually guided via finite element simulation, and the use of a scaled model test can not only verify the mechanical performance of the structure, but also preview and evaluate the actual control of the construction. The control of the accuracy of pylon deflection will affect the alignment of such long-span arch bridges [4], but there is little research available into pylon control (especially as related to the middle pier during cable-stayed suspension). At present, some Chinese researchers have studied the linear control of CFST arch bridges in different forms. Gu, Y [5] described arch rib construction technology to analyze arch rib installation control methods from the perspective of arch processing and the splicing of the steel tube based on the arch bridge characteristics and construction-control processes of CFST bridge types. Based on the grey prediction theory, Zhuo Xiaoli [6] established a grey model for line-shape prediction, considering the residual correction during the construction of main beams in the context of mid-span steel box arch bridges, and predicted the construction pre-elevation value of main beam segments through tower deviation. It can be seen that tower deflection and arch rib alignment in arch bridges interact [7–9]. The suspension assembly method is a common construction method for long-span arch bridges [10–12]. However, the studies on the suspension assembly method mainly focus on improving the accuracy of the cable forces [13], while the studies on tower deflection are few. At present, for a long-span steel truss arch bridge, suspension tower

construction is the most difficult and risky part of the construction process. The steel truss arch erection side span of the Jiangnan Seventh Bridge is installed by using the support method, and the middle span is installed via the cantilever method. The suspension tower plays an important role in the cantilever erection construction of the steel truss arch. The suspension tower is one of the key structures in the cantilever construction of the steel truss arch bridge, and it connects the cantilever end of the main arch with the balance end of the side beam using the suspension cable, so that the steel truss arch bridge can maintain overall stability during the construction of the main girder [14]. The application of monitoring technology to realize the construction-line monitoring of the suspension tower can not only meet the installation accuracy requirements of the suspension tower members, but also improve the safety and accuracy of subsequent main beam closure [15]. This issue has also been investigated by some foreign researchers in succession. In the large-span concrete arch bridge constructed via the cantilever pouring method [16], path control is key to ensuring construction quality, and the deflection of the buckle tower often affects the arch elevation of each segment. The influence of the deflection of the buckle tower on the elevation of each section during construction was analyzed via a geometric analysis method, and the finite element model was established in Midas software to verify the results. The results show that the deflection of the buckle tower has little effect on the elevation of the arch foot, but it has a greater effect on the elevation of the section near the arch top, and the section at the arch top is more sensitive to the change in the buckle-tower height. According to Jiang Wei [17], the structural state of the main cable of the hoisting system changes during the hoisting process. Based on the engineering background of a large bridge, this paper obtained a high-precision calculation method of the main cable sag and cable force during the hoisting process through theoretical deduction, and estimated the influence of vehicle traffic on the main cable force by numerical simulation. The results show that the proposed method for calculating the sag of the main cable has high accuracy and can be applied in practice. The main cable force increases gradually as the vehicle moves toward the mid-span and the main cable force at the pylon end reaches its maximum when the vehicle is within the span. Some scholars have also shown how to prevent the occurrence of tower deviations by monitoring via three-dimensional scanning, but they have not avoided the occurrence of tower deviations from the root.

In terms of the method of the tower deflection theory, Lin T.M. [18] used the suspension cable element method to derive a formula giving the deflection of the hinged tower of the cable hoisting system where the pressure tower is set, so that the calculation of the cable hoisting construction stage and the tower deflection calculation were unified. A feasibility control system of intelligent tower deviation was verified by theoretical analysis, but it has not been applied in engineering practice. Deng JiangMing [19] derived an analytical formula of the influence of the tower deflection with an integrated button-back on the linear arch rib by using a geometric analysis method. The feasibility of these proposed control systems as applied to intelligent tower deviation was validated by theoretical analysis, but the deformation of the tower is not considered.

In terms of calculation methods, Zhen-guo C et al. [20] considered the influence of the deflection of the buckle tower during the calculation of the cable force, and ascertained the that optimal buckle cable force matrix can be used to reduce the influence of buckle-tower deflection on the alignment of the arch rib. Ke-Jian Y [21] studied the sensitivity of each section of the buckle of the lower part of the buckle-tower to the vertical displacement of the closing hole, and found that too small a horizontal inclination would weaken the influence of the section buckle force on the vertical displacement of the closing hole, and they solved the problem of the low adjustment efficiency of the long buckle cable by calculating an optimal cable force via the formal installation iterative method. However, these two methods tend to be those viewed as lacking in innovation: if the number of iterations is excessive, the calculation will be slow. Xue-Tao D et al. [22] studied the influence of the main cable slip on tower deflection in the design of the cable hoisting system, and found that the main cable slip had a significant influence on the cable hoisting system, which

could significantly change the deviation of the top of the tower and the stress thereon. Wei S et al. [23] found that the displacement of the top of the tower in the integrated construction of cables and buckle towers exerts a significant influence on the accuracy of the arch-rib splicing, and the key to construction control is to reduce the deflection of the cable and the buckle tower. Therefore, the initial tension of the wind rope of the top cable should be adjusted while observing the deviation of the tower during the construction of the arch rib assembly, thereby reducing the horizontal cable force difference and keeping the cable and buckle tower in a vertical state as far as possible. The method is novel and unique in its technical aspects, but this method lacks theoretical support.

The safety and construction accuracy of the tower has been studied widely; taking the Changshou Yangtze River Bridge as the background, Gao Z [24] introduced the construction technology of a 60 m high, single-story, suspension tower from the design, construction, and to demolition. Taking the Nanjing Dashingguan Bridge as the background, Sheng Zhiping [25] innovatively laid a suspension tower with three layers of cable stays on the outside of the two-span steel beams, with a height of 68.5 m, and adopted flat cable construction technology on the inside, which overcame the problems of the internal force and alignment adjustment difficulty during the erection of steel beams. Zhi-Hu Z et al. [26], taking the Jiangnan Seventh Bridge as the background, conducted the stress analysis of various working conditions of the 89.6-m high sling tower during the assembly process. Renbo F et al. [27] studied the application of 39-m high suspension tower in flexible arch of a continuous steel girder in the Guanhe Super-Bridge on the Lianyan Railway. This long-span bridge has certain advantages and broad prospects for application. Due to its wide range of application, especially in long-span bridges, cable hoisting construction has become the main method of the erection of arch bridges [28–30]. When cables are used to lift arch ribs, the processes of each span affect the deformation of the tower, induce deviations, and have linking effects on the arch ribs suspended on the tower. When the linkage effect gradually accumulates, assembly accuracy and tower deviation will be affected if no adjustment is made [31,32]. In the present work, a set of new methods and theories are used to control tower deviation, limiting the occurrence of unbalanced tower deviation and the corresponding torsion at the root, which is different from the methods of other scholars. The problem of tower deviations is solved, and the accuracy of tower deviations is controlled to within the theoretical value, thereby achieving the ideal control effect.

2. Project Overview and Model Design

2.1. Project Overview

The Longtai Expressway is a section of China's national expressway network planning, which is one of the important links in the main skeleton expressway network planned across the Yangtze River, and is also the main channel from the central region to the south-east coast. The whole line adopts six-lane expressway standard construction. The Tianyun Bridge is one of the controlled, landscape-type, projects of the overall project. Its structure consists of two arch circles, three arch seats, middle piers and bridge panels. The main bridge adopts the main span of 2×260 m of a CFST to design the overall subgrade width of 16 m, the design load is Grade I (highway), and the structural safety grade is Grade I. The design speed is 80 km/h, and the bridge structure design life is 100 years. In the middle pier, there are buckle cables on both sides. Using the middle arch seat, sections are constructed on both sides at the same time, and the buckle cables are pulled up to complete its construction. The column on the arch adopts a row-type rectangular section structure, and the column is connected by a cross-beam. The span of the two-span continuous CFST intermediate truss arch is larger in the same type of bridge, the bridge continuously crosses the river, the bridge location on both sides of the mountains makes for difficult access to traffic, and its construction is difficult necessitating the present research into the key technology of design and construction. The general layout of the Tianyun Bridge is shown in (Figure 1).

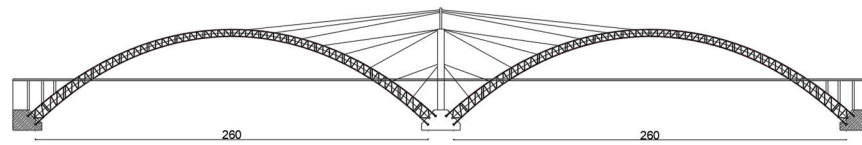


Figure 1. Layout of the Tianyun Bridge (unit: m).

2.2. Similarity Theory

For structural tests, it is most accurate to use the original actual structure for the simulation, so a certain proportion of model tests are often used, and the force state of the original structure is calculated through the use of the similarity ratio. To simulate the construction process of the Tianyuan Bridge, it is necessary to study the method used to control the tower deflection. To obtain more accurate test results and data, the geometric scaling ratio of the main arch ring, arch base and junction pier is proposed to be 1:10 on the basis of comprehensive consideration of the test content, model materials, production accuracy, and component volume, as well as considering time, economic cost, and data fidelity. The scale ratio of stress is 1:1, and the interface pier is designed in scale according to the ratio of pushing stiffness of 1:10.

From the scale ratio of geometry and force, the similarity coefficients are obtained according to the similarity theory as follows (Table 1):

Table 1. Model test similarity relationship.

Physical Quantity	Prototype	Model	Model Similarity Coefficient
Length	L_p	$L_m = L_p (1/n)$	1/10
Cross area	A_p	$A_m = A_p \cdot (E_p/E_m)$ $(1/n^2) (1/m)$	1/100
Bending moment of inertia	I_p	$I_m = I_p \cdot (E_p/E_m)$ $(1/n^4) (1/m)$	1/10,000
Torque moment of inertia	J_p	$J_m = J_p \cdot (G_p/G_m)$ $(1/n^4) (1/m)$	1/10,000
Modulus of elasticity	E_p	E_m	1
stress	σ_p	$\sigma_m = \sigma_p (E_p/E_m)$	1
strain	ε_p	$\varepsilon_m = \varepsilon_p$	1
Linear displacement	δ_p	$\delta_m = \delta_p \cdot (1/n)$	1/10
Angular displacement	α_p	$\alpha_m = \alpha_p$	1
counterweight	W_p	$W_m = W_p (1/n^2)$ $(1/m)$	1/100
Concentrated load	F_p	$F_m = F_p (1/n^2) (1/m)$	1/100
Shearing force	Q_p	$Q_m = Q_p (1/n^2)$ $(1/m)$	1/100
reaction	R_p	$R_m = R_p$ $(1/n^2) \cdot (1/m)$	1/100
Bending moment	M_{bp}	$M_{bm} = M_{bp} (1/n^3)$ $(1/m)$	1/1000
torque	MT_p	$MT_m = MT_p$ $(1/n^3) \cdot (1/m)$	1/1000

Note: In the table, n is the geometric scaling ratio (set to 10), and m denotes the scaling ratio of stress (set to 1).

2.3. Component Design

2.3.1. Arch Rib Design

According to the relevant design drawings of the Tianyun Bridge and the existing conditions, the values of the geometric similarity ratio of the main structural dimension are as per (Table 2).

Table 2. List of arch ring components (unit: mm) 30 September 2023.

Position	Original Bridge Dimension	Prototype Size	Model Size	Compressive Stiffness Ratio	Resistance to In-Plane Stiffness Ratio
Main chord 1	$\varphi 1600 \times 35$	$\varphi 80 \times 1.7$	$\varphi 36 \times 4$	1.02	1.04
Main chord 2	$\varphi 1600 \times 32$	$\varphi 80 \times 1.6$	$\varphi 35 \times 4$	1.2	1.11
Main chord 3	$\varphi 1200 \times 26$	$\varphi 70 \times 1.3$	$\varphi 35 \times 3$	1.1	1.12
Web rod 1	$\varphi 800 \times 20$	$\varphi 40 \times 1$	$\varphi 14 \times 4$	1.1	/
Web rod 2	$\varphi 600 \times 16$	$\varphi 30 \times 0.8$	$\varphi 15 \times 3$	1.2	/
Parallel connection 1	$\varphi 800 \times 20$	$\varphi 40 \times 1$	$\varphi 14 \times 4$	1.13	/
Parallel connection 2	$\varphi 800 \times 22$	$\varphi 40 \times 1.1$	$\varphi 12 \times 3$	1.15	/
Parallel connection 3	$\varphi 800 \times 16$	$\varphi 40 \times 0.8$	$\varphi 12 \times 3$	1.16	/
Cross-brace 1	$\varphi 800 \times 22$	$\varphi 40 \times 1.1$	$\varphi 14 \times 4$	1.13	/
Cross-brace 2	$\varphi 800 \times 16$	$\varphi 35 \times 1.1$	$\varphi 14 \times 4$	1.30	/
Cross-brace 3	$\varphi 700 \times 22$	$\varphi 40 \times 0.8$	$\varphi 12 \times 3$	1.09	/
Cross-brace 4	$\varphi 700 \times 16$	$\varphi 35 \times 0.8$	$\varphi 12 \times 3$	1.4	/
Fork stay	500×16	/	$\varphi 12 \times 2.6$	1.6	/

2.3.2. Arch Design

Due to this scaling model study, there are almost half spans on both sides. To make the scale model simulate the internal force and deformation of the real bridge, the arch design is strictly scaled down to ensure that the model undergoes no displacement in the construction and test process, which is aligned with reality. The arch seat diagram is shown in Figure 2.

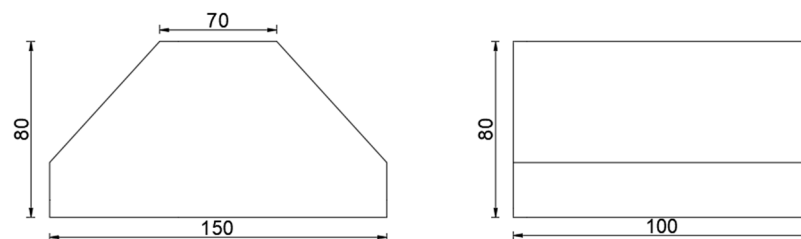


Figure 2. Arch abutment (unit: mm).

2.3.3. Pier Design

The height of the pier proposed in this design is 4.5 m + 1.5 m. The model test uses a steel tower pier (Figure 3).

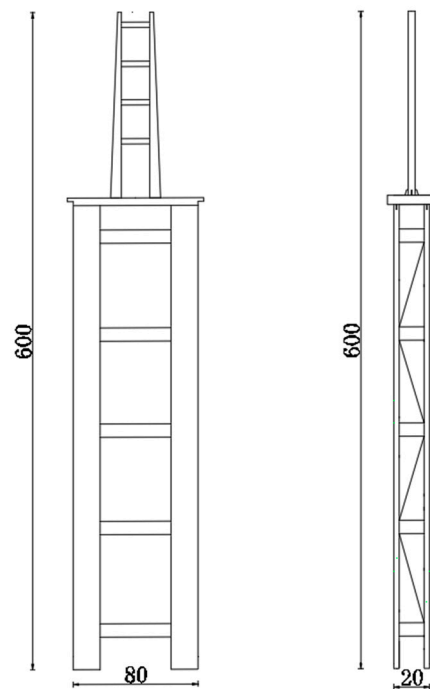


Figure 3. Intermediate pier (unit: mm).

3. Finite Element Analysis

3.1. Finite Element Model

The Midas finite element model is established based on the 1:10 scale model test. There are 2035 nodes and 3776 units in the whole bridge, among which the cable is a tension-only truss unit, and the main arch and tower are beam units. The simulation is conducted according to the hoisting sequence of the actual bridge during the construction stage.

For the convenience of description, the following is the partition diagram (Figure 4), for example: A2 is the second section of Side A.

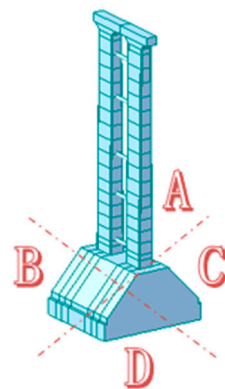


Figure 4. Azimuth zoning scheme.

3.2. Tower Deviation Calculation

The focus of the present research is the deviation of the middle pier tower. The deviation of the tower during normal construction is calculated: there are eight sections of the arch bridge, and some key sections are listed here, such as Section 2, Section 6, and Section 8. The outputs from the finite element analysis model are as follows:

Working condition 1: Hoisting arch rib A side of Section 2.

Working condition 2: Hoisting arch rib B side of Section 2.

In condition A2 (Figure 5), the unbalanced horizontal thrust is generated by unilateral lifting, with a 0.1 mm displacement at the bottom of the pier, a 0.88 mm displacement at

the mid-point of the pier, and a 1.6 mm displacement at the top of the pier. In condition B2 (Figure 6), due to the balanced horizontal thrust generated by lifting on both sides, there is almost no displacement at the top of the pier. The maximum stress on the bottom of the tower is 52 MPa.

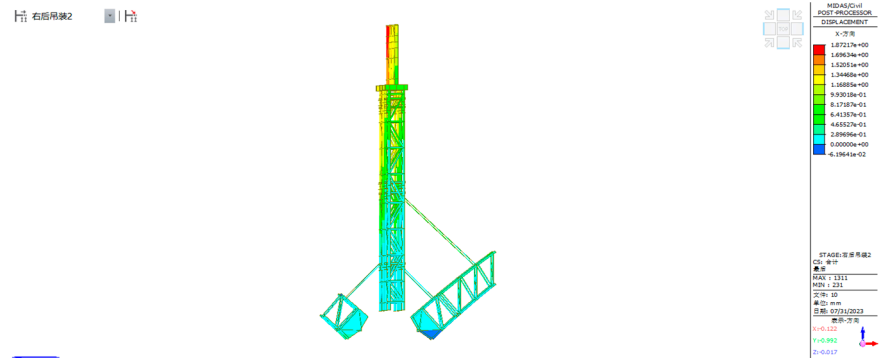


Figure 5. The second stage tower deviation (A2).

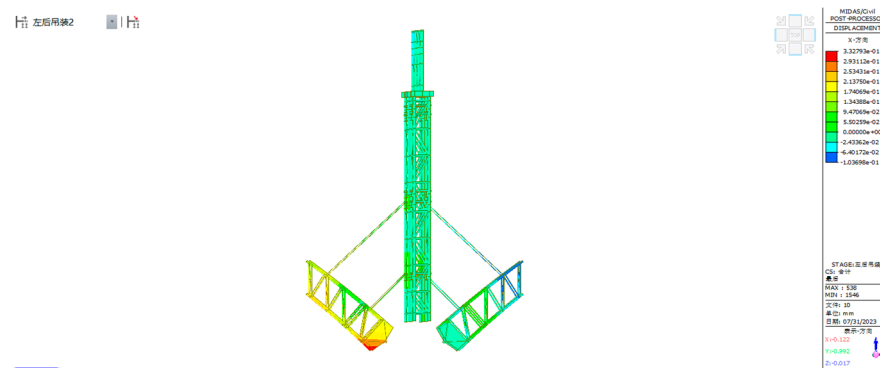


Figure 6. The second stage tower deviation (B2).

Working condition 3: Lifting Section 6 on side D of the arch rib.

Working condition 4: Lifting Section 6 on side C of the arch rib.

In condition D6 (Figure 7), the unbalanced horizontal thrust is generated by unilateral lifting. The displacement at the bottom of the pier is 0.1 mm, the displacement at the middle of the pier is about 0.9 mm, and the displacement at the top of the pier is 2.51 mm. In condition C6 (Figure 8), due to the balanced horizontal thrust generated by lifting on both sides, there is almost no displacement at the top of the pier. The maximum stress on the bottom of the tower is 82 MPa.

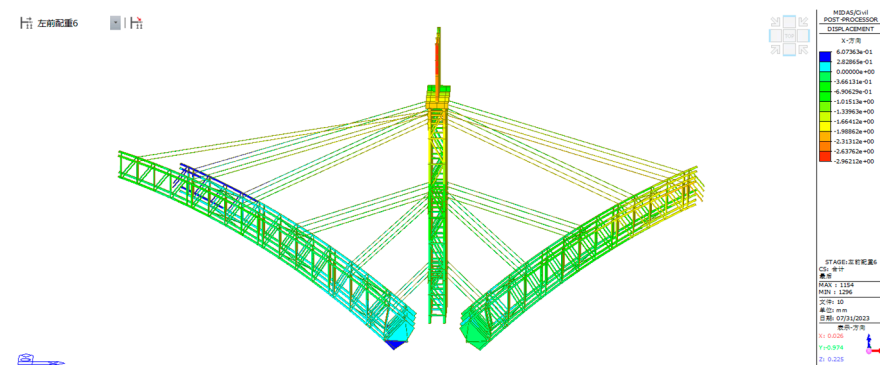


Figure 7. The sixth stage of tower deviation (D6).

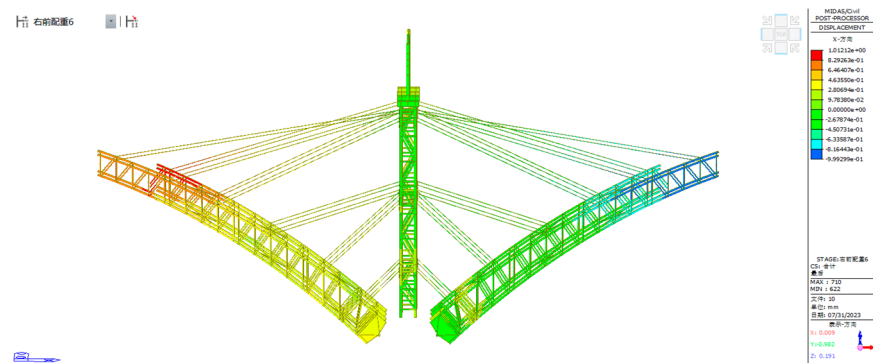


Figure 8. The sixth stage of tower deviation (C6).

Working condition 5: Lifting Section 8 on side A of the arch rib.

Working condition 6: Lifting Section 8 on side B of the arch rib.

In condition A8 (Figure 9), the unbalanced horizontal thrust is generated by unilateral lifting. The displacement at the bottom of the pier is 0.1 mm, the displacement at the middle of the pier is about 0.78 mm, and the displacement at the top of the pier is 2.85 mm. In condition B8 (Figure 10), due to the balanced horizontal thrust generated by lifting on both sides, there is almost no displacement at the top of the pier. The maximum stress on the bottom of the tower is 118 MPa.

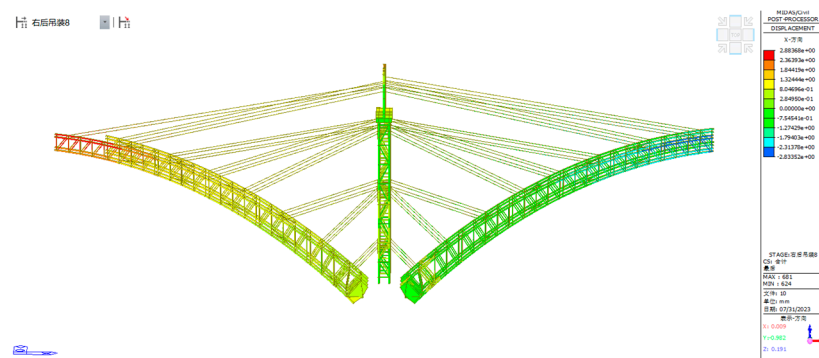


Figure 9. The eighth stage of tower deviation (A8).

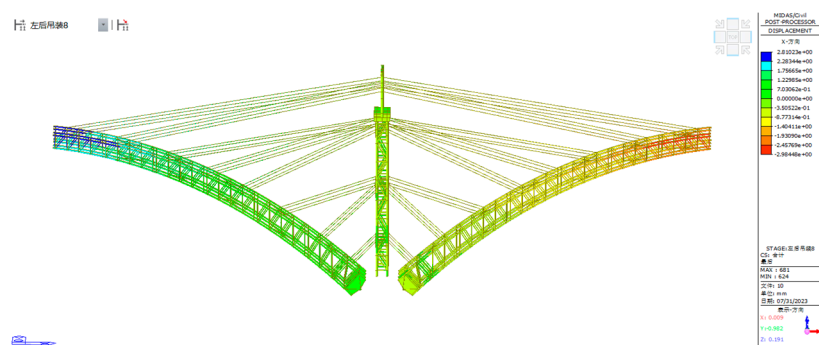


Figure 10. The eighth stage of tower deviation (B8).

The column deviation data under a normal construction sequence are listed below; these lay a foundation for the comparison of the data of new construction methods.

4. New Methods of Control Theory

4.1. Control Method

In this method, the single-side segment and the arch rib segment on the symmetrical side are hoisted first, the cable is not initially tensioned, the unbalanced bending moment

is borne via the existing cable-stayed cable system, and the rear tensioned cable is used as a protective device. The aforementioned steps are repeated, and the two rear ends are symmetrically tensioned at the same time, which can ensure the reduction in tower deviation and the torsion caused by the single-side asymmetric hoisting problem (Figure 11)

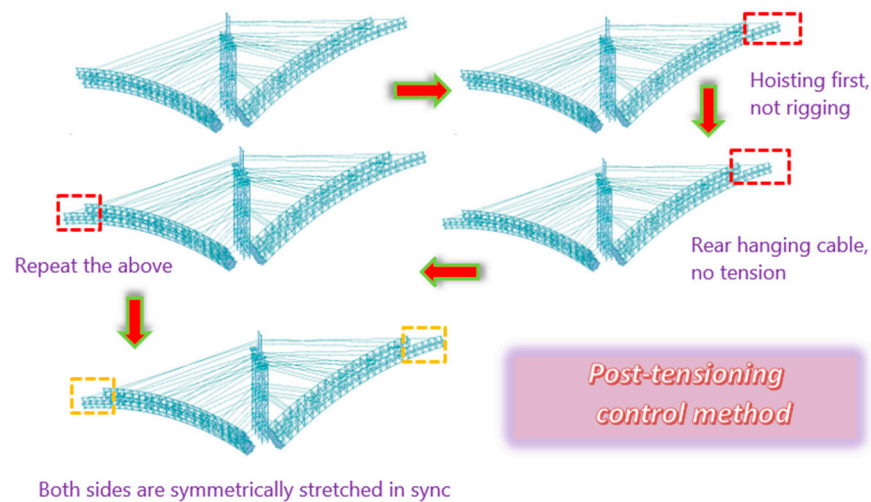


Figure 11. The method used to control tower deviation.

4.2. Tower Deviation Analysis

The following experimental results can be obtained: the first seven sections of the experiment are constructed in the form of the unilateral installation and tightening of segment buckle cables, and the other side is the same. Section 8 adopts the construction method of lifting on both sides first, not tightening the cable, and pulling the cable on both sides at the same time after the symmetrical segment is installed. The following table shows the deviation data for the traditional hoisting of segments 2 and 6, and the deviation data for segment 8 using the new method. T1 is the measurement point at the bottom of the tower, T2 is the measurement point in the middle of the tower, and T3–T6 are the four measurement points at the top of the tower (Figure 12).

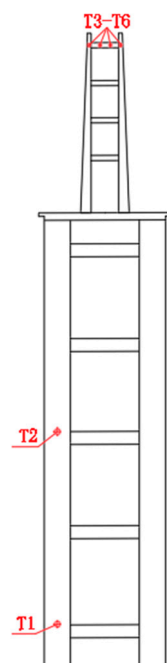


Figure 12. Measuring points T1 to T6.

In Tables 3 and 4, Δx is the longitudinal deviation of the bridge from the tower, Δy is the transverse deviation of the bridge from the tower, and Δz is the elevation change, indicating the change in the tower deviation on the hoisting side of the segment. $\Delta x'$ is the longitudinal deflection of the bridge towards the tower, $\Delta y'$ is the transverse deflection of the bridge towards the tower, and $\Delta z'$ is the elevation change, and the change in deflection of the mounting buckle tower on the other side of the symmetric segment. Measurements are made via total station. Tables 3 and 4 list the traditional tensioning column deviation data.

Table 3. Section 2 tower deviation (unit: mm).

	Δx	Δy	Δz	$\Delta x'$	$\Delta y'$	$\Delta z'$
T1	0.0006	0.0002	0.0004	0.0017	0.0003	−0.0002
T2	0.0018	0.0006	0.0014	0.0010	−0.0003	0.0002
T3	0.0048	0.0005	0.0021	0.0009	−0.0005	0.0008
T4	0.0031	0.0008	0.0005	0.0000	0.0002	−0.0002
T5	0.0021	0.0004	0.0005	−0.0010	−0.0001	−0.0011
T6	0.0009	0.0002	0.0001	−0.0026	−0.0003	−0.0004

Table 4. Section 6 tower deviation (unit: mm).

	Δx	Δy	Δz	$\Delta x'$	$\Delta y'$	$\Delta z'$
T1	−0.0001	0.0003	−0.0004	0.0003	0.0002	−0.0002
T2	−0.0005	−0.0003	−0.0003	0.0005	0.0006	0.0002
T3	−0.0020	−0.0005	0.0006	0.0009	0.0005	0.0008
T4	−0.0025	0.0002	−0.0001	0.0010	0.0008	−0.0002
T5	−0.0027	−0.0001	−0.0012	0.0014	0.0004	−0.0011
T6	−0.0047	−0.0003	−0.0007	0.0016	0.0002	−0.0004

Tables 5 and 6 list the column deviation data of the eighth stage after adopting the new tensioning method.

Table 5. Section 8 tower deviation (unit: mm).

	Δx	Δy	Δz	$\Delta x'$	$\Delta y'$	$\Delta z'$
T1	−0.0002	0.0003	−0.0004	0.0003	0.0002	0.0002
T2	−0.0010	−0.0009	−0.0003	0.0005	−0.0003	0.0004
T3	−0.0042	−0.0006	0.0006	0.0009	0.0008	0.0006
T4	−0.0037	−0.0005	−0.0001	0.0010	−0.0002	−0.0002
T5	−0.0030	0.0002	−0.0012	0.0010	0.0009	−0.0009
T6	−0.0025	−0.0008	−0.0007	0.0011	0.0008	−0.0004

Table 6. Section 8 tower deviation (unit: mm).

	Δx	Δy	Δz	$\Delta x'$	$\Delta y'$	$\Delta z'$
T1	0.0003	0.0002	0.0002	−0.0002	−0.0002	−0.0002
T2	0.0006	0.0005	0.0005	−0.0004	0.0003	0.0002
T3	0.0011	0.0004	0.0016	−0.0007	−0.0004	0.0008
T4	0.0009	0.0005	0.0006	−0.0006	−0.0002	−0.0002
T5	0.0007	0.0006	0.0001	−0.0007	0.0002	−0.0011
T6	0.0005	0.0003	0.0000	−0.0006	0.0005	−0.0004

5. New Methods of Optimization Data Analysis

Using data comparison, it can be found that the transverse deviation of the tower is insignificant, and most of the deviation is within 0.5 mm, so there is little scope for the description and calculation of the transverse deviation therein. The working conditions of

A2, B2, and Section 6 are given in Figure 13, and the data pertaining to both the simulation and experiment are compared. To improve practicability, the maximum stress of the arch foot of the two methods corresponding to the section is listed (Figure 13).

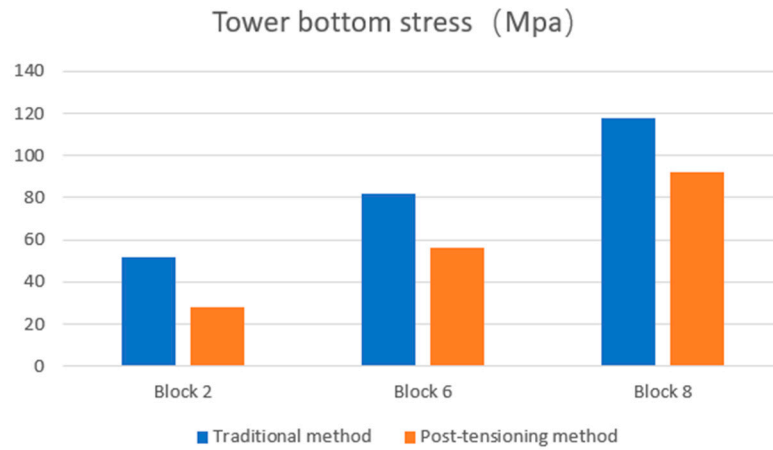


Figure 13. Comparison of arch-foot stress between the two methods.

It can be seen above that the method of the back cable can reduce the stress on some arch feet, and that on the eighth section, it can be reduced by about 25%. The following is a comparison of the actual and theoretical data of each section, and the last two charts allow the comparison of the data of the post-cable and traditional methods (Figures 14–19).

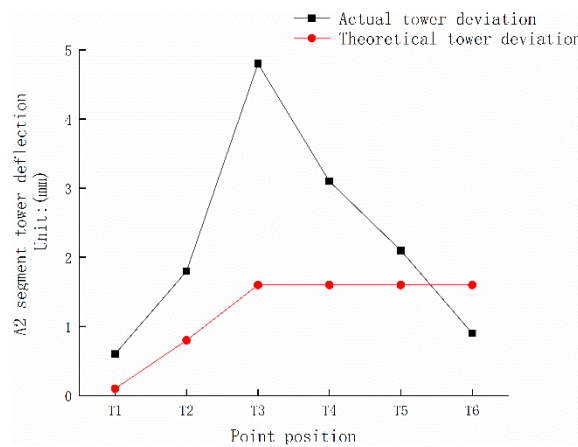


Figure 14. Section 2 tower bias comparison.

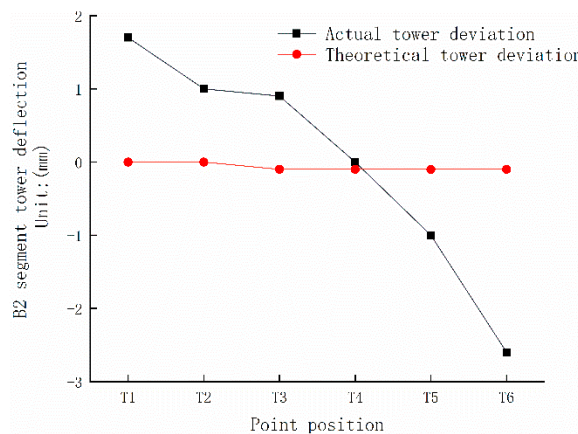


Figure 15. Section 2 tower bias comparison.

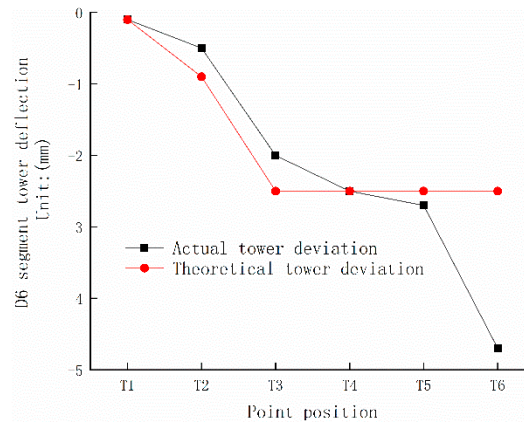


Figure 16. Section 6 tower bias comparison.

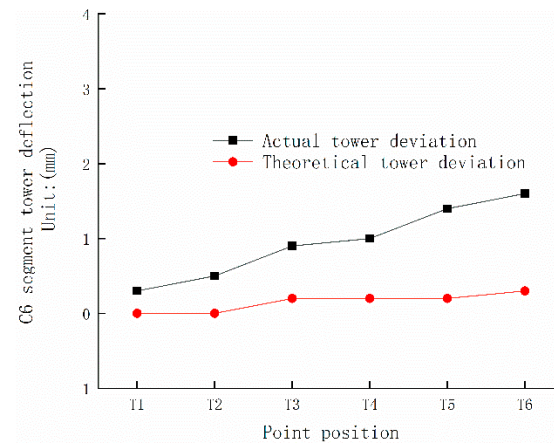


Figure 17. Section 6 tower bias comparison.

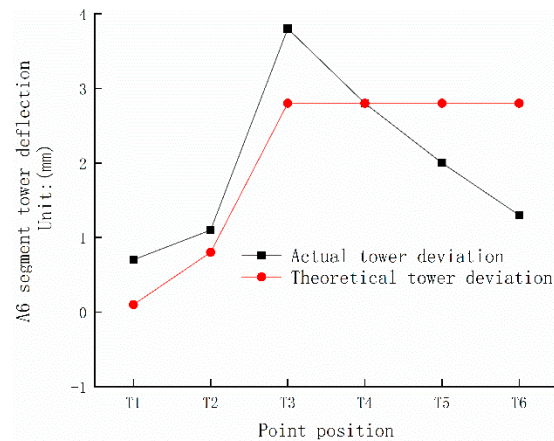


Figure 18. Section 6 tower bias comparison.

It can be seen that the traditional method induces asymmetric column deviation control and torsion problems. The actual data indicate that T3–T6 is the control point at the top of the buckle tower, and the actual data differ greatly, so the effect of lifting the unilateral rear cable is poor.

The following new method is applied to Section 8: after hoisting two symmetrical segments, both sides are tensioned at the same time, and the data are compared with that collected when hoisting one side segment at a time (Figures 20 and 21).

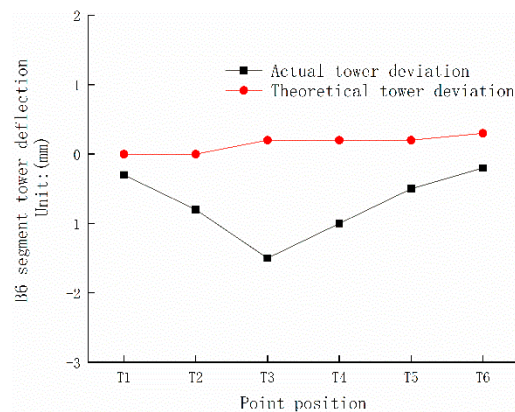


Figure 19. Section 6 tower bias comparison.

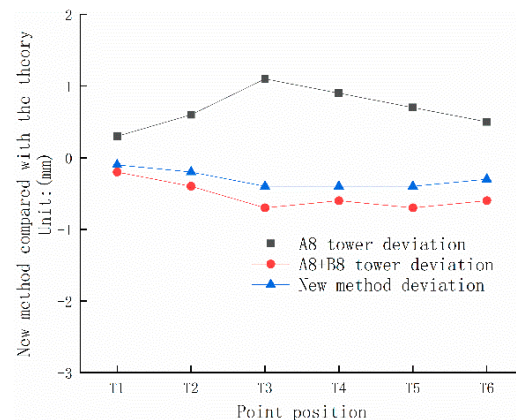


Figure 20. The new method is compared with the traditional method (A8 + B8 sides).

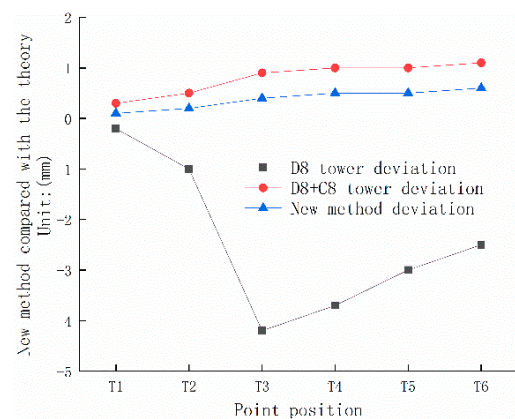


Figure 21. The new method is compared with the traditional method (C8 + D8 sides).

The comparison of the pictures shows that this method can actively and timeously correct the displacement deviation of the tower top and the torsion on the symmetric segment during the cable hoisting process, reducing the deviation. The maximum deviation of the tower pier can be controlled, in real time, to within the range of ± 0.5 mm.

6. Conclusions

To study the effect and operation of the new method of tower deflection control on the deflection of the buckle tower, and to apply it to the universality of similar bridge projects, the following conclusions can be drawn by establishing a 1:10 scale model:

- (1) The deflection of the buckle tower increases with the increase in the number of arch-rib lifting segments and the increase in pier elevation, from the bottom to the top of the tower;
- (2) The traditional way of controlling the deviation of the tower body is to pull a lot of steel wire and jack manually, which wastes a lot of materials and manpower. The new proposed method relies on the simultaneous tensioning technique, thereby greatly reducing the time cost, and obviating the need to adjust the offset;
- (3) After adopting the new method, the influence of adjusting the tower deviation on the structure members is rendered insignificant. This means that the adjustment has a significant controlling effect on the longitudinal displacement of the tower, and can reduce the stress on the arch foot; each section analyzed benefitted from a stress reduction of about 30 MPa compared with the previous method;
- (4) This method can actively and timeously correct the displacement deviation of the top of the tower and the torsion in the symmetric segment in the process of cable hoisting, reducing the deviation. The maximum deviation of the tower pier can be controlled, in real time, within the range of ± 0.5 mm. Compared with the traditional methods and techniques, the results can provide a reference for the deviation control of the middle pier tower of similar types of bridge.

Author Contributions: X.D., methodology and finite element analysis, drawing and translation; D.Y., editing and modification. All authors have read and agreed to the published version of the manuscript as submitted.

Funding: This research received no external funding.

Data Availability Statement: The data are available on request only due to commercial restrictions.

Conflicts of Interest: The authors declare no conflict of interest.

References

1. Yazhou, X. Structural Study of Arch Bridge With a Span of 600 m Part I: Trial Design. *Appl. Mech. Mater.* **2011**, *138*, 300–304.
2. Zhang, F. Study on Filling Sequence of Long-Span Concrete-Filled Steel Tube Arch Ribs and Hydration Heat of Concrete in Pipes. Master's Thesis, Chongqing Jiaotong University, Chongqing, China, 2020.
3. Ma, Y. Application and development of concrete-filled steel tube arch bridge. *Eng. Res.* **2019**, *4*, 212–213.
4. Wang, F.; Zheng, W.; Liu, H. Determination and Control of Alignment in Construction of CFST Arch Bridge. *Technol. Highw. Transp.* **2021**, *37*, 98–104+110.
5. Gu, Y.; Li, Y.D.; Liu, S.Z. Research on Construction Control of Long-span CFST Arch Bridge. *Appl. Mech. Mater.* **2015**, *777*, 88–93. [[CrossRef](#)]
6. Zhuo, X. Research on Construction Alignment Control of Main Girder of Half-Through Steel Box Arch Bridge Based on Grey Theory. *J. Highw. Eng.* **2021**, *46*, 26–32+67.
7. Zheng, J.L.; Wang, J.J. Concrete-Filled Steel Tube Arch Bridges in China. *Engineering* **2017**, *4*, 143–155. [[CrossRef](#)]
8. Chen, B.C.; Wang, T.L. Overview of Concrete Filled Steel Tube Arch Bridges in China. *Pract. Period. Struct. Des. Constr.* **2009**, *14*, 70–80. [[CrossRef](#)]
9. Han, L.H.; Li, W.; BJORHOVDE, R. Developments and advanced applications of concrete-filled steel tubular (CFST) structures: Members. *J. Constr. Steel Res.* **2014**, *100*, 211–228. [[CrossRef](#)]
10. Gao, X.; Liu, L.J.; Yao, S.K.; Yang, J.W.; Li, Y. Commonly Encountered Damages in Cable Members of CFST Arch Bridge and Detection Methods. *Key Eng. Mater.* **2012**, *619*, 71–80. [[CrossRef](#)]
11. Zhang, Z.-C.; Ye, G.-R.; Cheng, H.-Z. Calculation of SBC forces for concrete-filled steel tubular arch bridge with long span in process of lifting. *J. Zhejiang Univ. Eng. Sci.* **2004**, *38*. [[CrossRef](#)]
12. Zhou, Q.; Zhou, J.T.; Ma, H.; Li, X.-G.; Zhang, L. Improved algorithm of cable force for one time cable tensioning on steel tube arch ribs with segmental hoisting. *J. Traffic Transp. Eng.* **2020**, *20*, 92–101.
13. Zhou, Q.; Zhou, J.T.; Chen, J.W.; Feng, Y. Improved algorithm of cable force optimization of one—Time tensioning for arch bridge. *J. Fuzhou Univ. Nat. Sci. Ed.* **2019**, *47*, 412–416.
14. Liang, D.; Zhao, K. Virtual Steel Pylon Segments Assembly Method Based on 3D Laser Scanning. *Bridge Constr.* **2019**, *51*, 62–71.
15. Tian, W.; Liu, D. Closure Technique for Steel Truss Arch and Girder of the Second Hengqin Bridge in Zhuhai. *World Bridges* **2016**, *44*, 31–35.
16. Wu, P.; Pan, R.; Guo, J. Study on Influences of Phlon Displacement on Arch Rib Elevation of Concrete Arch Bridge Using Cantilever Casting Method. *J. Railw. Eng. Soc.* **2020**, *254*, 154–158.

17. Jiang, W.; Li, X. High Precision Calculation of Structural State of Main Cable during Cable Lifting Construction of Steel Tube Arch Bridge. *J. China Foreign Highw.* **2020**, *252*, 123–127.
18. Lin, T.M.; Zhong, Q.S.; Li, S.R. Segmental catenary method of calculating the cable curve of suspension bridge. *J. China Railw. Soc.* **2003**, *25*, 87–91.
19. Deng, J. Geometrical Analysis of Arch Rib Elevation Change Caused by Tower Deviation during Cable-Hoisting Construction. *J. Chongqing Jiaotong Univ. Nat. Sci.* **2009**, *3*, 505–508.
20. Cheng, Z.G.; Bai, Y.H.; Liu, C.T. The Control of Tower Deviation on Arch Installation in Xiaohe Grand Bridge. *Technol. Econ. Areas Commun.* **2010**, *3*, 87–89.
21. Yang, K.J.; Li, F.Q.; Zhang, Y.L. Research on the Design of Large Span Deck Steel Tube Concrete Arch Bridge. *J. Railw. Eng. Soc.* **2008**, *25*, 66–71.
22. Deng, X.T.; Zeng, D.R.; Zhou, Y.Q. Finite Element Analysis of Stability of Cable-Hoisting Erection System of Long-Span Arch Bridge. *J. Chongqing Jiaotong Univ. Nat. Sci.* **2007**, *26*, 1–5.
23. Shen, W.; Zhang, Y.Z.; Wen, L.U. Construction Control Method of Long-Span Steel Box Tied Arch Bridge. *West. China Commun. Sci. Technol.* **2009**, *12*, 85–89.
24. Gao, Z. Traveling wave effect of multi-span through concrete-filled steel tubular arch bridge. *J. Vibroengineering* **2022**, *24*, 19. [[CrossRef](#)]
25. Sheng, Z. Construction of Fastening Stay Tower at Pier No. 8 of Dashengguan Changjiang River Bridge in Nanjing. *Bridge Constr.* **2010**, *2*, 5–9.
26. Zhu, Z.H.; Lun, Y.I.; Gao, Z.Y. Analysis of Mechanical Behavior and Study of Construction Control Measures of Triple Main Truss Structure of Dashengguan Changjiang River Bridge in Nanjing. *Bridge Constr.* **2009**, *3*, 28–32.
27. Feng, R.; Zhao, H.; Tailei, C. Key Construction Techniques of Main Span Steel Truss Girder Flexible Arch of Guanhe Super-Long Bridge on Lianyungang-Yancheng Railway. *Railw. Eng.* **2017**, *8*, 47–49.
28. John, J.S. Construction of the Hoover Dam Bypass. *Concr. Int.* **2010**, *33*, 30–35.
29. Wei, J.; Chen, B. Application and research advancement of long span concrete arch bridges abroad. *World Bridge* **2009**, *2*, 4–8.
30. Shi, W.Z.; Ko, J.M.; Zhao, C.Y.; Chen, L. A bridge structural health monitoring information system based on GIS and DBMS. In Proceedings of the International Society for Optics and Photonics, San Diego, CA, USA, May 2005.
31. Yong, H.E.; Miao, Y.F.; Liu, H. Based on Beidou/GPS precise displacement monitoring technology in the application of the bridge monitoring. *J. Yunnan Univ. Nat. Sci. Ed.* **2016**, *38*, 35–39.
32. Wu, J.-C.; Wang, Z.-C.; Shi, X.-Y. Application of Beidou Satellite Communication and Positioning Technology to the Field Geological Survey in Northwestern China. *J. Geomech.* **2012**, *18*, 282–287.

Disclaimer/Publisher’s Note: The statements, opinions and data contained in all publications are solely those of the individual author(s) and contributor(s) and not of MDPI and/or the editor(s). MDPI and/or the editor(s) disclaim responsibility for any injury to people or property resulting from any ideas, methods, instructions or products referred to in the content.